Spectroscopic investigation of metal content in pre-strike arc during making operation in a low-current model switch

Naghme Dorraki, Kaveh Niayesh, *Senior Member, IEEE*

***Abstract* — Energy dissipation during pre-strike arc is the critical factor for electrical contacts erosion and welding in medium voltage load break switches. Using air-filled devices as an alternative to SF_6, makes the switch environmentally friendly, but leads to a more challenging process due to a higher pre-strike arcing time between contacts. Therefore, understanding the erosion process of electrical contacts is crucial to improve the switch lifetime. Determination of contacts surface evaporation by optical emission spectroscopy is one of the most precise methods to investigate the pre-strike arc interface with the contacts. In this paper, the temporal and spatial profiles of copper and tungsten emitted species during pre-strike arc are presented. For this purpose, a circuit consisting of a synthetic DC high voltage part is used to initiate the arc. The temporal evolution of CuI, CuII, and WI shows evaporation of the cathode and the anode surfaces during the pre-strike arc, and the spatial profiles show an inhomogeneous distribution of the vapors alongside the arc root.**

***Index Terms*—Arcing contacts, arc erosion, contacts evaporation, Load break switch, Medium voltage, Optical emission spectroscopy.**

I. Introduction

With power system development, there are more demands to cut costs. Circuit breaker as one of the primary devices in electrical networks to make, carry, and break the current in normal and abnormal operating conditions, have high maintenance costs due to several types of stresses, ageing and reliability requirements [1]. Medium voltage Load break switches (MV-LBS) could be an inexpensive alternative to circuit breakers in distribution networks [2]. There are several studies on current interruption for MV-LBS in order to improve and design environmentally friendly and cost-effective switches like compact air-based LBS [2, 3]. Beside current interruption, which is typically limited to less than 1kA, MV-LBS should be able to withstand a number of making operations under short-circuit currents of several tens of kilo amperes while avoiding severe contact degradation [4, 5]. Under fault conditions, the switch must be able to close the contacts at any time without welding them together and re-open for the next operation. Therefore, practical condition assessment is necessary to improve the stability and lifetime of MV-LBS regarding contacts erosion and degradation [4, 6].

Erosion of electrical contacts in making operation starts before the contacts touch due to a dielectric breakdown. Therefore, the switching is initiated from the pre-strike arc ignition, which can take up to a few milliseconds before contacts touch. The dissipated energy is partly absorbed by contacts surfaces and can heat them up to the melting and evaporation point, eventually leading to their welding. Even if contacts are separable for the next operation, the eroded surfaces could increase ohmic losses in the close position when current flows and rises the temperature while a low resistance is necessary to obtain a high rated load current [4]. Contacts erosion, because of heating up the surfaces, depends on some parameters, including arc energy, arc time, and material properties. Using air-based MV-LBS instead of SF_6 makes the switchgear environmentally friendly. Unfortunately, it also leads to a more challenging making operation due to a higher arcing time in air because of the lower dielectric strength compare to SF_6 [2, 7, 8].

Among several studies that have been done to investigate electrical contacts erosion during switchgear operation [8-14], arc spectroscopy can provide detailed information of contacts erosion as a result of arc interface [15, 16]. The interface of thermal arc plasma and electrical contacts surfaces causes evaporation of the contacts surfaces. Depending on the material of the contacts and the arcing energy, formed metal vapors can have a significant influence on the arc dynamic motion and properties [17, 18]. The relatively low ionization potential of such additives compared to atomic gases like oxygen and nitrogen modifies the arc conductivity and temperature [19, 20]. Temporal evolution and spatial distribution of metal vapors by optical emission spectroscopy (OES) could pave the way for a better understanding of contacts erosion due to arcing in switchgears.

The pre-strike arc with load current could be dominated by metal vapors [21]. The influence of metal vapors on arc

N. Dorraki and K. Niayesh are with the Department of Electric Power Engineering, Norwegian University of Science and Technology, 7491 Trondheim, Norway. (e-mail: naghme.dorraki@ntnu.no)

characteristics have been studied on free burning arc and arc welding by OES [20, 22]. Some unexpected findings have resulted like temperature fall in the center of arc due to the presence of metal vapors. These results emphasize the importance of a systematic investigation on determining the impact of critical parameters like metal vapors on arc dynamic motion and stability in MV-LBS. This study is a part of a systematic investigation of contacts erosion during making operation in MV-LBS.

There are some limitations in OES measurements for high intense light of the arc as optically thick plasma. Besides, the pre-strike arc burns in the first few milliseconds of currents starting from zero, and the majority of the current passes through the contacts in closed position. Therefore, the systematic investigation started with low-current arc to get an insight into the behavior of pre-strike arc with the highest spatial resolution. For this purpose, a test object with a spring-type drive mechanism is employed to simulate making operation, and an optical emission spectroscopy set-up is designed to record the temporal evolution and spatial profile of metal vapors while contacts are approaching.

II. Experimental Set-up and Methods

A schematic of the experimental arrangement consisting of the test circuit and the optical measurement system is shown in Figure 1. This circuit is a part of the full synthetic making circuit based on the IEC 62271-101 standard.

A. Test Circuit

The test circuit includes a 0.7 µF high voltage capacitor (C). The capacitance is selected in such a way that the discharge current doe not decay after few tens of microseconds and an arc still exists, so that the main current can flow through the pre-strike arc. The capacitor can be charged to a predefined charging voltage up to 20 kV through a resistor (R_1). Once the capacitor is fully charged to a selected voltage, switch S_1 is opened to disconnect the charged capacitor from the high voltage power supply. When a breakdown occurs between the closing contacts of the test object, the fully charged capacitor is discharged through resistor R_2 and further through the test object.

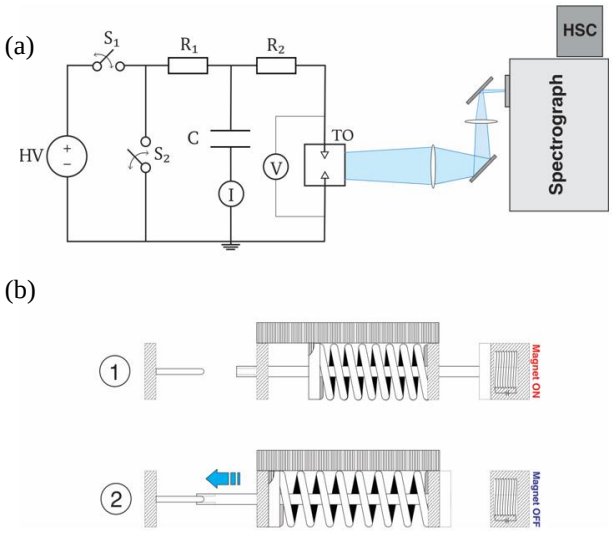

Figure 1. Schematic of the experimental set-up. (a) the test circuit and optical diagnostic set-up, (b) spring-type test object; (1) open and (2) close position

A Pearson current sensor measures the arc current. To avoid the interference of electromagnetic noises, an optical system transmits the measured data to record them [16, 23, 24].

The test object (TO) is a spring-type switch with axisymmetric arcing contacts (Figure 1(b)). The stationary contact (anode) is a pin with a diameter of 6 mm, and the dynamic one (cathode) is a tulip with an outer diameter of 15 mm. The electrical contacts are made of copper-tungsten (20/80), and the closing velocity is 3 m/s. The closing speed and the material type are chosen so that they do not differ too much from the commercial product.

B. Optical measurement

The time evolution of contacts evaporation together with spatial profiles under arc formation are recorded and analyzed employing video spectroscopy. In comparison with other methods for OES, video spectroscopy can provide information on both temporal evolution of different atoms, ions, and neutrals transitions and their spatial profiles simultaneously during a recording.

The spectroscopic set-up (Figure 1(b)) consists of a spectrograph with a 300 mm focal length with a 600 lines/mm grating (Princeton Instrument Acton SP-300i) and a high-speed camera (Photron fastcam mini UX50) with 1280×1024 pixel matrix to record the time evolution of pre-strike arc. The set-up is aligned in 1.2 m from the anode with 26.2 pixel/mm spatial resolution. For all the measurements, the spectrograph slit is set alongside the arc root to obtain quantitative information on metal vapor distribution between the contacts with a focus on the anode.

III. Results

In this section, the interface of arc and anode surface is investigated by electrical measurement and optical emission spectroscopy, which includes both time-resolved and spatial-resolved spectroscopy.

A. Electrical characteristics

To make the pre-strike arc, the capacitor is charged to 18.5 kV and connected to the anode. The arc burns between contacts while the closing operation is performed and the contacts are approaching. Experiments are carried out to study the effect of arcing time on contacts degradation at low currents. Two different pre-strike arc durations are chosen by setting the discharge resistor R2. The current waveforms are shown in Figure 2 (b). The current amplitude starts at 200A for the current profile 1 and decays to almost zero within 270 µs, and the current profile 2 begins at 80A and lasts for 600 µs. Travel-curve of the dynamic contact could reveal the condition of the operating mechanism. Figure 2 (a) shows the travel-curve profile of the moving contact (i.e. cathode). At the time of 31.88 ms, the arc is ignited, and the cathode has reached the anode at 33.84 ms.

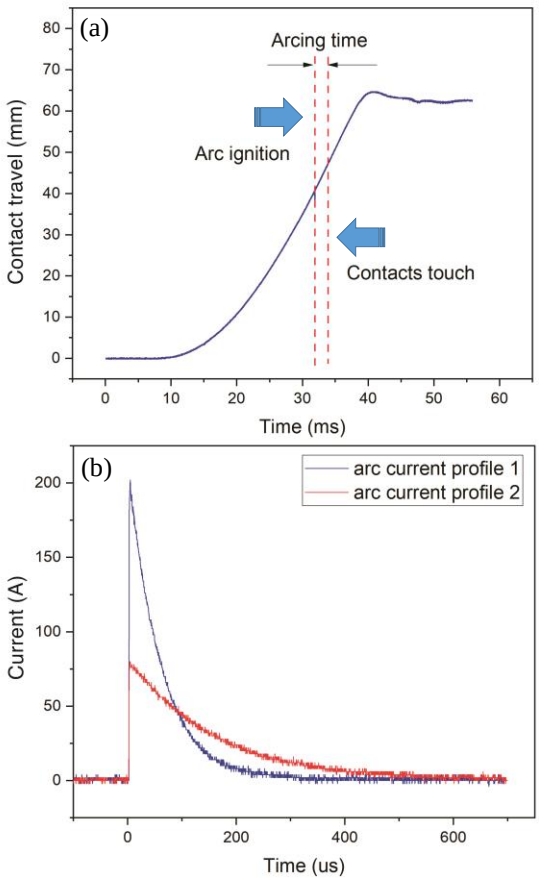

Figure 2. (a) Travel-curve profile of the dynamic contacts, (b) arc current waveforms

B. OES

1) Spectral Bandwidth

To get information on which species are emitted during the pre-strike arc, a series of two-dimensional spectra is recorded with a spectral resolution of ~0.4 nm, recording speed of 40000 fps and an exposure time of 20 µs. The arc current profile 1 is applied for this series of recording. Since the probability of copper emissions is higher than tungsten due to their physicochemical characteristics, the spectral range of 473-538 nm is chosen, which is dominated by atomic and ionic spectral emission lines of copper. Figure 3 shows the observation window of the spectrometer and an example of the recorded 2-D spectral emission lines at 0.4 nm spectral resolution. For temporal evolution analysis, 1-D spectrum is chosen at the

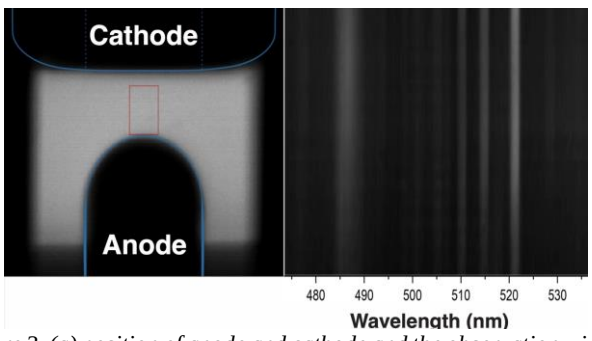

Figure 3. (a) position of anode and cathode and the observation window for recording 40000 fps and 0.4 nm spectral resolution. (b) an example of the spectral lines.

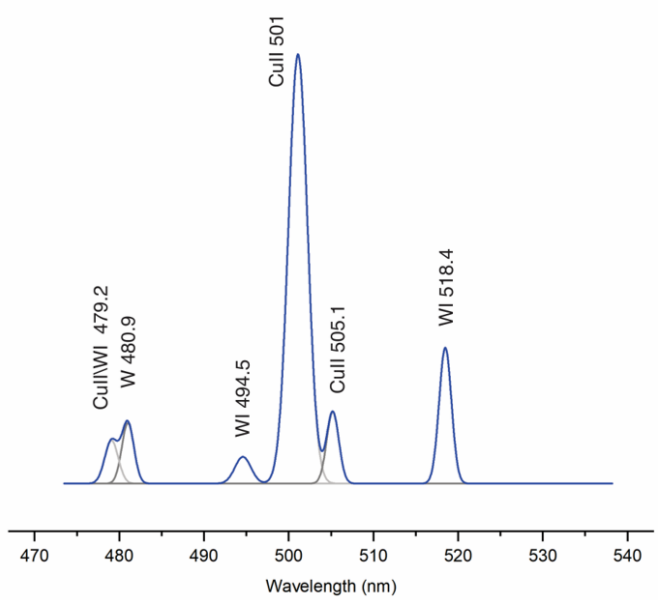

Figure 4. Spectral profile from 2 mm above anode at 25 µs.

position of ~2 mm above the pin (anode) where the maximum intensity of emission lines is reached. The wavelength bandwidth is chosen around 505 nm, where copper spectral lines dominate the emissions. However, some emission lines of tungsten and hydrogen beta Balmer line (Hβ) are also detected.

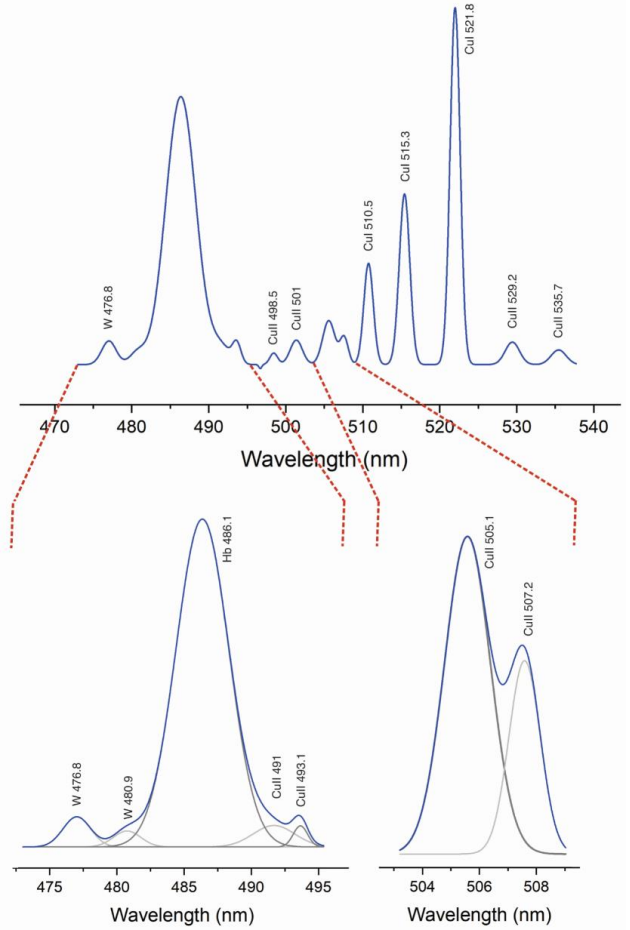

Figure 5. Spectral profile at 100 µs with peak fitting for two overlapped sections.

TABLE 1
WAVELENGTH OF ATOMIC AND IONIC EMISSION LINES USED IN THIS WORK

Species	Wavelength (nm)
CuI	510.5, 515.3, 521.8
CuII	491, 493.1, 501, 505.1, 507.2, 535.7, 529.2
WI	494.5, 518.4
Hβ	486.1
*Undefined**	479.2, 480.9, 476.8

*Close transition levels made it impossible to distinguish some species between WI/II and CuII

Recorded spectral lines in the first 25 µs of the arcing show a different type of species emission lines compared to the rest of arcing time. Figure 4 shows well-resolved spectral lines for this moment. The spectrum is achieved by Gaussian peak fitting with Chi-Square tolerance value of 10^{-9} after baseline correction. For comparison, the same correction applied to all the spectra. The wavelengths related to the recorded emission lines are chosen based on NIST Atomic Spectra Database and earlier studies [25, 26]. The most intense ionic copper lines (CuII) are observed at 501, 505.1, and 529.2 nm. Three atomic spectral lines of WI are recorded at 518.4, 494.5, and 480.9 nm. Another spectral emission line is observed at 479.2 nm, which could be CuII or WI. Due to the close transition of copper and tungsten at this wavelength and the spectral resolution, it is not possible to distinguish between them.

In the recorded spectra after 25 µs of the arcing, there is no sign of tungsten emission lines at 476.8, 480.9, 494.2, and 518.4 nm. Figure 5 shows the spectrum at 75 µs after the arc starts. The same correction method used in Figure 4 is applied here. There are sharp copper atomic lines at 510.5, 515.3, and 521.8 nm that are known to have very high transition probabilities and are often used for temperature analysis [24, 27]. Some of the ionic transition lines of copper are detected at 535.7, 507.2, 505.1, 501, 498.5, and 529.2 nm which are weaker than atomic ones. The hydrogen beta Balmer line Hβ is appeared at 486.1 nm, and because of its strong intensity has an overlap with two ionic emission lines of copper (491 and 493.1 nm) and the emission line of tungsten (480.9 nm). Figure 5 shows the peak fitting around 486 and 506 nm to distinguish peaks from the overlaps. The emission of atomic and ionic metal species are due to electrical contacts ablation and erosion since there is no other metallic source in the test object and the Hβ spectral line emission is observed because of the breakdown in the air as the dielectric medium of the switch. A summary of detected wavelengths is presented in Table 1.

Based on the obtained results and bandwidth limitation for video spectroscopy, distinctive copper atomic lines at 510.5 and 521.8 nm are chosen for this study due to their high intensity and the low probability to overlap with other lines. For this purpose, the center wavelength is set to 515.3 nm. Recording speed of 80000 fps with an exposure time of 10 µs and spectral resolution of ~0.65 nm are chosen.

2) Time evolution:

For the sake of reproducibility of the experiments, several tests have been done. The spectrum showed in Figure 4 is not observed on all the tests. Since the exposure time to record this spectrum is less than 20 µs, the reason for not finding the same first spectrum for all the tests could be a time-mismatch between the high-speed camera triggering and the arc ignition. Therefore, the first spectrum with emission lines at 510.5 and 521.8 nm is considered as the start of the temporal evolution of metals emission in the pre-strike arc which could have a delay

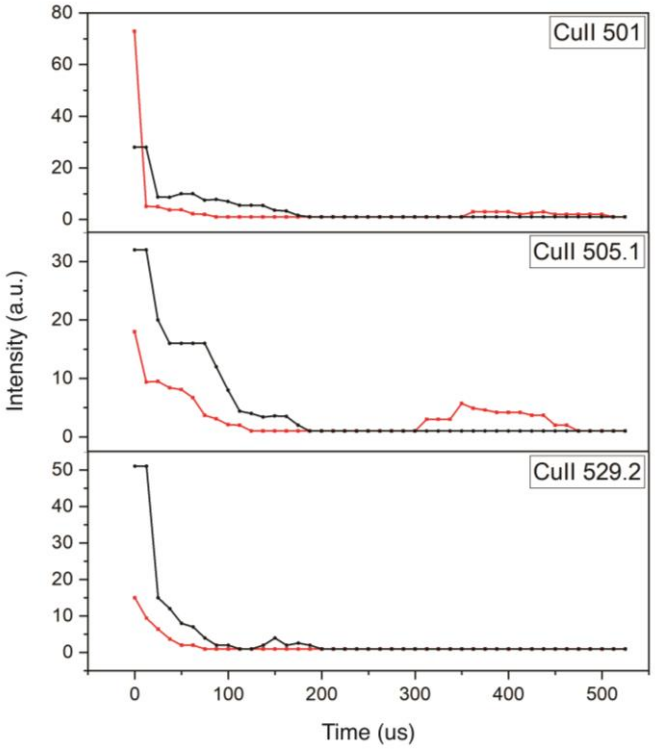

Figure 6. Temporal distribution copper ionic emissions. Black and red lines represent arc current profiles 1 and 2, respectively.

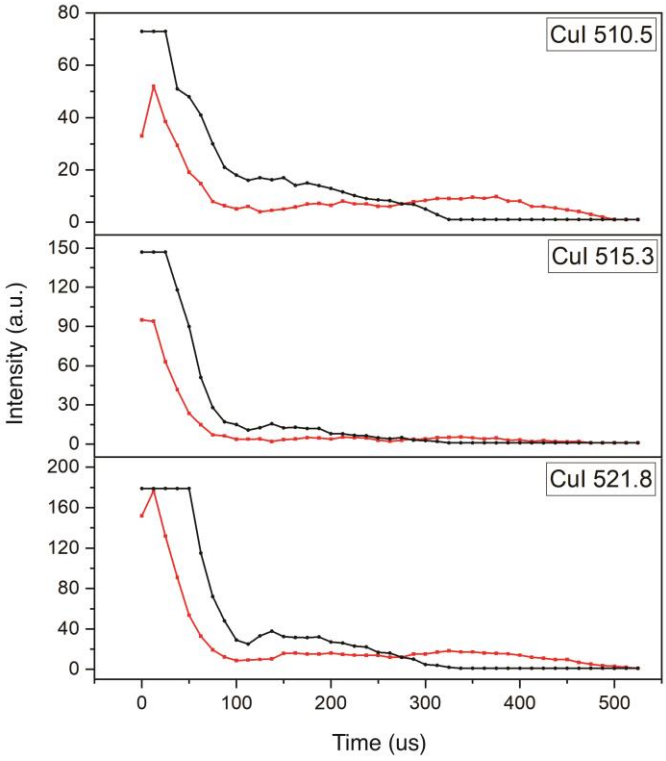

Figure 7. Temporal distribution of copper atomic emissions. Black and red lines represent arc current profile 1 and 2, respectively.

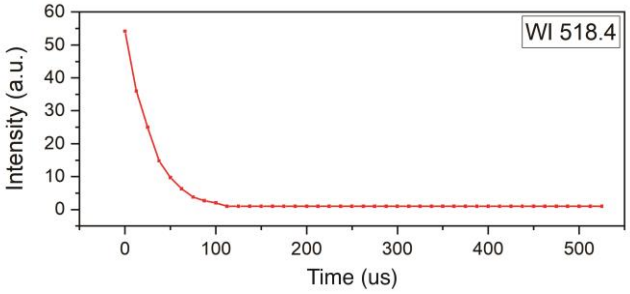

Figure 8. Temporal distribution of tungsten atomic emission at 518.4 nm for the arc current profile 2

less than 12.5 µs to the arc ignition.

Temporal distribution of copper atomic and ionic lines are shown in Figure 6 and Figure 7, respectively, for two different arc current profiles at 2 mm above the anode. Similar copper emission lines are observed in all performed experiments with approximately the same intensity ratio. It has to be mentioned that for the current profile 1, the emission lines intensities are saturated in the first ~12.5 µs for all the species, ~40 µs for 510.5 and 515.3 nm, and ~60 µs for 521.8 nm. The values in the curves at these moments are undefined and reported based on the next unsaturated measurable emission line.

The results indicate that the emission of copper atomic lines are dominating in the contacts gap. They show longer lifetimes and higher intensities compared to ionic ones. During the pre-strike arc, all the lines intensities decrease considerably. Still, there is a slight increase in copper atomic lines intensities for the arc current profile 1 after 130 µs and both atomic and ionic lines intensities for the arc current profile 2 after 350 µs.

Regarding tungsten atomic emissions, the emission lines are not intense enough to be visible during arcing except the emission at 518.4 nm. This spectral line is observed in case of the arc current profile 2. The temporal distribution is shown in Figure 8.

3) Spatial profile:

For a better understanding of metal vapor distribution in the gap, the spatial profile of copper atomic emission at 521.8 nm is investigated. Figure 9 shows recorded images at 1.5 mm above the anode surface at different arcing times for both arc current profiles. The horizontal white dashed line in the middle of images shows the position that is chosen for the temporal investigation of metal vapors in the previous section. As shown in temporal evolution, there is an increase in emission intensities of the species. Images 2-4 in Figure 9 give a better view of copper vapor intensity increase in the 2-D distribution profile. Image 3 shows the maxima at 112.5 µs and 350 µs for the arc current profiles 1 and 2, respectively.

IV. Discussion

Tungsten copper alloy as the material of the electrical contacts in this study has an amorphous refractory microstructure, which consists of 80% tungsten and 20% copper. The contacts have both high conduction of Cu and high erosion resistance of W. Due to the higher conductivity of copper, pre-strike arc usually hits the copper regions to initiate, otherwise the arc formation causes tungsten ablation to pass current. This erosion effect can be seen on the recorded spectrum at the first 25 μs of the arcing time, as shown in Figure 4. As mentioned before, a number of tests have been done to confirm the reproducibility of the emitted pieces. In some of the tests, the first recorded spectrum is different from the rest of the spectra. The presence of a sharp emission peak of atomic tungsten at 518.4 nm and two other emission lines in the first 25 μs and the difference in plasma composition at this time to the rest of the arcing time confirm ablation of tungsten. Also, the emission at 518.4 nm continues during arc burning in just a few of the recordings, which could be the same reason explained and randomly chosen region on the surface of the contact to initiate arc burning, which also depends on the grain size of copper and tungsten.

The time evolution of metal vapor intensities recorded in the selected observation window close to the anode surface shows the highest relative concentrations (Figure 9-1) at the peak of arc currents. For the first 60 µs at the wavelength of 521.8 nm, the emitted light was highly intense and saturated for spectral lines in current profile 1. At the same time, for current profile 2 the emission intensities are measurable. The metal vapor intensities decrease exponentially until a specific time that a slight increase observed. At this moment, the current is about few amperes while the metal vapor emissions increase. The analysis of this increase has to be done taking into account the thermal inertia of metallic contacts and the travel curve of the dynamic contact (the cathode), which is shown in Figure 2 (a).

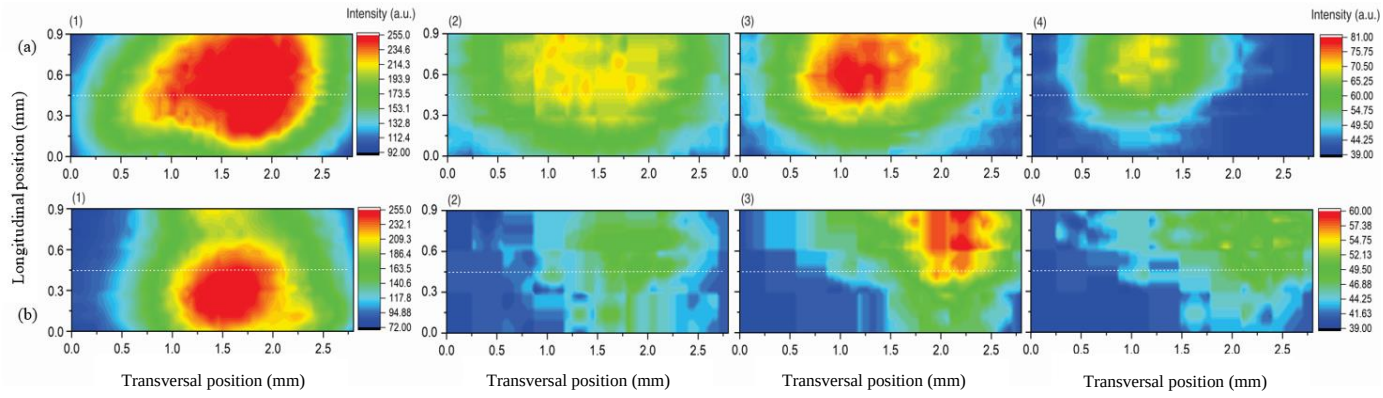

Figure 9. 2-D distribution of copper vapor (521.8 nm) at anode for the arc current profile 1 (a) at 50 µs (1), 112.5 µs (2), 137.5 µs (3), and 412.5 µs (4) and for the arc current profile 2 (b) at 25 µs (1), 162.5 µs (2), 350 µs (3), and 412.5 µs (4).

There is a time delay in temperature rise of metallic surfaces to evaporation point when they are exposed to heat caused by arcing. Since the intensity increase is observed on top-half of the observation window, the thermal inertia could not be the only reason for the intensities increase; otherwise, the growth has to be seen from the closest position to the contact surface.

In closing the switch with the speed of 3 m/s, the arc is ignited when the contacts are at a distance of 7 mm, and the spatial distribution of copper vapor (Figure 9) shows high vapor concentration close to the arc axis. Therefore, the increase could be as a result of either the cathode surface evaporation, which is transferred to the observation window due to contacts approaching or a part of the copper vapor evaporated from the anode surface that is returned to the observation window. It can be seen that the metal species last for a longer time in current profile 2, considering the increase in relative emission intensity compared to current profile 1, which shows the effect of longer arcing time in species distribution.

The presence of metal vapors could affect arc transport properties, particularly conductivity due to the low value of the ionization potential of the metal atoms and arc temperature fall due to radiative emissions[19, 22, 28]. The spatially resolved distribution of metal content makes it possible to trace particles in the arc column. The first 50 µs of arcing time shows the highest concentration of metal content for both current profiles at copper atomic emission lines, which is diffused afterward, and a fraction of metallic particles move across arc axis, as shown in Figure 9. This observation contrasts some computational studies that showed no displacement of metal vapors when the arc current is lower than one kA [29, 30].

In the case of higher current, the distribution of metal vapors could significantly change the pre-strike arc parameters during making operation, which may cause problems with maintenance and reliability of the switching device. The obtained results in this study on the distribution of metal vapors could facilitate a detailed understanding of the pre-strike arc behavior in making operation to improve the lifetime of such devices.

V. Conclusion

The presence and transport of metallic particles as a result of arc-electrical contacts interface have been investigated by optical emission spectroscopy for two different currents with different arcing time. The analysis of the time evolution of metal content during the pre-strike arc shows tungsten ablation and inhomogeneous distribution of copper vapors in the axis of the pre-strike arc without observing any changes in decaying arc current profiles. In addition, spatially resolved distribution of copper vapors shows high diffusion of particles during the first 50 µs of the arcing time and transport a fraction of metal particles in the arc column.

The results of this study provide support for computational studies on low-current arc. Furthermore, the investigation on low current pre-strike arc could be used to clarify metal vapor distribution at higher currents in MV-LBS due to limitations for OES measurements for thick plasma. This study must be continued by applying a higher current to investigate pre-strike arc characteristics (thermal and electrical behavior) and estimate the electrical contacts erosion process.

Acknowledgment

The work was financially supported by the Norwegian Research Council, grant # 269361. The authors would like to thank Erik Jonsson from SINTEF energy research and Bård Ålmos and Morten Flå from NTNU for technical supports.

References

[1] Z. Zhang, J. Zhang, E. Gockenbach, and H. Borsi, "Life management of SF 6 circuit breakers based on monitoring and diagnosis," *IEEE Electrical Insulation Magazine*, vol. 25, no. 3, pp. 21-29, 2009.

[2] N. S. Støa-Aanensen, M. Runde, E. Jonsson, and P. D. Teigset, "Empirical relationships between air-load break switch parameters and interrupting performance," vol. 31, no. 1, pp. 278-285, 2016.

[3] H. Taxt, K. Niayesh, and M. Runde, "Self-Blast Current Interruption and Adaption to Medium-Voltage Load Current Switching," *IEEE Transactions on Power Delivery*, vol. 34, no. 6, pp. 2204-2210, 2019.

[4] K. Niayesh and M. Runde, *Power Switching Components*. Springer, 2017.

[5] M. Seeger, "Perspectives on research on high voltage gas circuit breakers," *Plasma Chemistry and Plasma Processing*, vol. 35, no. 3, pp. 527-541, 2015.

[6] M. Mohammadhosein, K. Niayesh, A. A. Shayegani-Akmal, and H. Mohseni, "Online assessment of contact erosion in high voltage gas circuit breakers based on different physical quantities," *IEEE Transactions on Power Delivery*, vol. 34, no. 2, pp. 580-587, 2018.

[7] E. Jonsson and M. Runde, "Interruption in air for different medium-voltage switching duties," *IEEE Transactions on Power Delivery*, vol. 30, no. 1, pp. 161-166, 2014.

[8] J. Tepper, M. Seeger, T. Votteler, V. Behrens, and T. Honig, "Investigation on erosion of Cu/W contacts in high-voltage circuit breakers," *IEEE transactions on components and packaging technologies*, vol. 29, no. 3, pp. 658-665, 2006.

[9] P. G. Slade, *Electrical contacts: principles and applications*. CRC press, 2017.

[10] F. Pons and M. Cherkaoui, "An electrical arc erosion model valid for high current: Vaporization and Splash Erosion," in *2008 Proceedings of the 54th IEEE Holm Conference on Electrical Contacts*, 2008: IEEE, pp. 9-14.

[11] S. Zhu, Y. Liu, B. Tian, Y. Zhang, and K. Song, "Arc erosion behavior and mechanism of Cu/Cr20 electrical contact material," *Vacuum*, vol. 143, pp. 129-137, 2017.

[12] F. Pons, M. Cherkaoui, I. Ilali, and S. Dominiak, "Evolution of the AgCdO contact material surface microstructure with the number of arcs," *Journal of electronic materials*, vol. 39, no. 4, pp. 456-463, 2010.

[13] S. B. Wang *et al.*, "Electrical Erosion Characteristics of Pt-Ir-Zr Alloy Contact under DC Load," in *Applied Mechanics and Materials*, 2013, vol. 395: Trans Tech Publ, pp. 191-195.

[14] Y. Wu *et al.*, "Visualization and mechanisms of splashing erosion of electrodes in a DC air arc," *Journal of Physics D: Applied Physics*, vol. 50, no. 47, p. 47LT01, 2017.

[15] K. Hartinger, L. Pierre, and C. Cahen, "Combination of emission spectroscopy and fast imagery to characterize high-voltage circuit breakers," vol. 31, no. 19, p. 2566, 1998.

[16] A. Khakpour *et al.*, "Video spectroscopy of vacuum arcs during transition between different high-current anode modes," *IEEE Transactions on Plasma Science*, vol. 44, no. 10, pp. 2462-2469, 2016.

[17] A. Belinger, N. Naudé, J. Cambronne, and D. Caruana, "Plasma synthetic jet actuator: electrical and optical analysis of the discharge," *Journal of Physics D: Applied Physics*, vol. 47, no. 34, p. 345202, 2014.

[18] F. Valensi *et al.*, "Plasma diagnostics in gas metal arc welding by optical emission spectroscopy," *Journal of Physics D: Applied Physics*, vol. 43, no. 43, p. 434002, 2010.

[19] X. Li, H. Zhao, and A. B. Murphy, "SF6-alternative gases for application in gas-insulated switchgear," *Journal of Physics D: Applied Physics*, vol. 51, no. 15, p. 153001, 2018.

[20] A. B. Murphy, "Influence of metal vapour on arc temperatures in gas–metal arc welding: convection versus radiation," *Journal of Physics D: Applied Physics*, vol. 46, no. 22, p. 224004, 2013.
[21] S. Franke, R. Methling, D. Uhrlandt, R. Bianchetti, R. Gati, and M. Schwinne, "Temperature determination in copper-dominated free-burning arcs," *Journal of Physics D: Applied Physics*, vol. 47, no. 1, p. 015202, 2013.
[22] A. B. Murphy, "The effects of metal vapour in arc welding," *Journal of Physics D: Applied Physics*, vol. 43, no. 43, p. 434001, 2010.
[23] A. Khakpour *et al.*, "Investigation of anode plume in vacuum arcs using different optical diagnostic methods," *IEEE Transactions on Plasma Science*, vol. 47, no. 8, pp. 3488-3495, 2019.
[24] A. Khakpour *et al.*, "Time and space resolved spectroscopic investigation during anode plume formation in a high-current vacuum arc," *Journal of Physics D: Applied Physics*, vol. 50, no. 18, p. 185203, 2017.
[25] https://physics.nist.gov/PhysRefData/ASD/lines_form.html.
[26] J. Pettersson, M. Becerra, S. Franke, and S. Gortschakow, "Spectroscopic and Photographic Evaluation of the Near-Surface Layer Produced by Arc-Induced Polymer Ablation," *IEEE Transactions on Plasma Science*, vol. 47, no. 4, pp. 1851-1858, 2019.
[27] A. Khakpour, R. Methling, S. Franke, S. Gortschakow, and D. Uhrlandt, "Vapor density and electron density determination during high-current anode phenomena in vacuum arcs," *Journal of Applied Physics*, vol. 124, no. 24, p. 243301, 2018.
[28] M. Schnick, U. Füssel, M. Hertel, A. Spille-Kohoff, and A. Murphy, "Metal vapour causes a central minimum in arc temperature in gas–metal arc welding through increased radiative emission," *Journal of Physics D: Applied Physics*, vol. 43, no. 2, p. 022001, 2009.
[29] J. L. Zhang, J. D. Yan, and M. T. Fang, "Electrode evaporation and its effects on thermal arc behavior," *IEEE Transactions on Plasma Science*, vol. 32, no. 3, pp. 1352-1361, 2004.
[30] A. Kadivar and K. Niayesh, "Two-way interaction between switching arc and solid surfaces: distribution of ablated contact and nozzle materials," *Journal of Physics D: Applied Physics*, vol. 52, no. 40, p. 404003, 2019.

Naghme Dorraki received the B.Sc. degree in optics and laser engineering from University of Tabriz, Iran, in 2011, and the M.Sc. degree in photonics from Laser and Plasma research institute, Shahid Beheshti University, Tehran, Iran, in 2015. She is currently pursuing a Ph.D. degree in with the Department of Electric Power Engineering Norwegian University of Science and Technology (NTNU), Trondheim, Norway.

Kaveh Niayesh completed the B.Sc. and M.Sc. degree in Electrical Engineering from the University of Tehran, Iran, in 1993 and 1996 respectively. In 2001, he completed the Ph.D. degree from the RWTH-Aachen University of Technology in Electrical Engineering. In the last 19 years, he held different academic and industrial positions including Principal Scientist with the ABB Corporate Research Center, Baden-Dättwil, Switzerland; Associate Professor with the University of Tehran; and Manager, Basic Research, with AREVA T&D, Regensburg, Germany. Currently, he is a Professor in the Department of Electric Power Engineering at Norwegian University of Science and Technology (NTNU), Norway. His research interests are mainly in the broad field of high voltage and switchgear technology; specifically on current interruption in power switching devices in AC and DC power networks, breakdown and aging behavior of insulation materials exposed to HVDC and repetitive fast impulses, as well as diagnostic and condition assessment of power switchgear.